Ultrafast non-adiabatic dynamics of methyl substituted ethylenes: The π3s Rydberg state

Cite as: J. Chem. Phys. **135**, 164309 (2011); https://doi.org/10.1063/1.3652966
Submitted: 01 April 2010 . Accepted: 12 September 2011 . Published Online: 28 October 2011

Guorong Wu, Andrey E. Boguslavskiy, Oliver Schalk, Michael S. Schuurman, and Albert Stolow

Ultrafast non-adiabatic dynamics of methyl substituted ethylenes: The π3s Rydberg state

Guorong Wu, Andrey E. Boguslavskiy, Oliver Schalk, Michael S. Schuurman, and Albert Stolow[a)]

Steacie Institute for Molecular Sciences, National Research Council, 100 Sussex Dr., Ottawa, Ontario K1A 0R6, Canada

(Received 1 April 2010; accepted 12 September 2011; published online 28 October 2011)

Excited state unimolecular reactions of some polyenes exhibit localization of their dynamics at a single ethylenic double bond. Here we present studies of the fundamental photophysical processes in the ethylene unit itself. Combined femtosecond time-resolved photoelectron spectroscopy (TRPES) and *ab initio* quantum chemical calculations was applied to the study of excited state dynamics in *cis*-butene, *trans*-butene, trimethylethylene, and tetramethylethylene, following initial excitation to their respective π3s Rydberg states. The wavelength dependence of the π3s Rydberg state dynamics of tetramethylethylene was investigated in more detail. The π3s Rydberg to $\pi\pi^*$ valence state decay rate varies greatly with substituent: the 1,2-di- and tri-methyl substituted ethylenes (*cis*-butene, *trans*-butene, and trimethylethylene) show an ultrafast decay ($\sim$20 fs), whereas the fully methylated tetramethylethylene shows a decay rate of 2 to 4 orders of magnitude slower. These observations are rationalized in terms of topographical trends in the relevant potential energy surfaces, as found from *ab initio* calculations: (1) the barrier between the π3s state and the $\pi\pi$* state increases with increasing methylation, and (2) the π3s/$\pi\pi$* minimum energy conical intersection displaces monotonically away from the π3s Franck-Condon region with increasing methylation. The use of systematic methylation in combination with TRPES and *ab initio* computation is emerging as an important tool in discerning the excited state dynamics of unsaturated hydrocarbons. [doi:10.1063/1.3652966]

I. INTRODUCTION

Ethylene is the smallest organic molecule containing a carbon-carbon double bond. Its behavior upon photoexcitation often serves as a model for understanding photochemical and photobiological processes in larger molecules, particularly their reaction dynamics,[1] including the fundamental process of *cis-trans* isomerization. For example, theoretical calculations show that the photodynamics of ethylene shares similarities with dynamics in the much larger 1,2-diphenylethylene (stilbene).[2–4] Indeed, some unsaturated hydrocarbons, such as butadiene,[5] cyclopentadiene,[6,7] and cyclohexa-1,4-diene,[8] appear to localize their excited state dynamics on the ethylenic subunit even though their UV chromophores are quite delocalized. This suggests that a systematic study of the effect of chemical substitution on the excited state dynamics of ethylene may provide further insights into the applicability and limitations of ethylene as a model for the larger unsaturated hydrocarbons. In this paper, we present studies on the effects of methyl substitution on the dynamics of the π3s Rydberg state. In a subsequent paper, we will present our studies on the effects of methyl substitution on the dynamics of the $\pi\pi^*$ state.

We begin with a brief review of the excited state dynamics of ethylene itself. The electronic ground state of ethylene is planar and stable with respect to twisting. Its absorption spectrum begins around 200–210 nm and reaches a broad maximum near 162 nm (7.65 eV), where it is, however, superimposed with very sharp structures.[9–12] The strong and broad electronic transition is attributed to the $\pi\pi^*$ state, whereas the sharp structures were assigned to the π3s Rydberg state. In Mulliken's nomenclature,[10] the $\pi\pi^*$ state is called the V (valence excited) state, the π3s Rydberg state is called the R state, and N (normal) denotes the ground state.

The substituted ethylenes studied here are 1,2-dimethylethylene (*cis*-butene, *trans*-butene), trimethylethylene, and tetramethylethylene. Upon increasing methylation, the origin of the π3s$\leftarrow$N transition shifts strongly to the red (as does the ionization potential), whereas the V$\leftarrow$N transition maximum shifts only slightly to the red.[10,13–15] As a result, the π3s$\leftarrow$N bands, which in ethylene lie fairly close to the V$\leftarrow$N Franck-Condon (FC) maximum, move relatively further to the red with methylation, until in tetramethylethylene, they are clearly isolated from the V$\leftarrow$N transition. For 1,2-dimethylethylene and trimethylethylene, the π3s$\leftarrow$N bands may be overlapped with the red edge of the strong V$\leftarrow$N bands. In general, the spectra of these substituted ethylenes are diffuse, prohibiting a facile decomposition.

Fluorescence studies and high-resolution excited-state photoelectron spectroscopy studies have provided information about the excited states involved.[16–19] The lifetimes of some mono-olefinic hydrocarbons were estimated[16] from integrated oscillator strengths of the electronic transitions, fluorescence quantum yields, and their concentration-dependent

a)Author to whom correspondence should be addressed. Electronic mail: albert.stolow@nrc.ca.

quenching by CCl_4 or O_2. For *cis*- and *trans*-butene vapour excited at 184.9 nm, the estimated lifetimes were in the 10–100 fs range. For tetramethylethylene vapour (∼125 Torr and 25 °C), the excited state lifetime at 228.8 nm was estimated to be about 4 ps, whereas at 184.9 nm, it was 3 to 4 times shorter. An R→N assignment for the emission was proposed for all these molecules. The low fluorescence quantum yield was proposed as being due to ultrafast non-radiative decay of the R to V state for *cis*- and *trans*-butene, whereas for tetramethylethylene, intersystem crossing from a singlet to a triplet Rydberg state was suggested.[16] Wickramaaratchi and co-workers performed fluorescence quantum yield studies of tetramethylethylene under collisionless condition, yielding a strongly excitation wavelength dependent lifetime which was determined to be 20.8 ± 0.9 ns upon excitation at 235 nm.[17] No conclusive identification of the emitting state was given. In 1990s, Siebrand *et al*. showed that the fluorescence excitation spectrum of tetramethylethylene can be vibrationally resolved in a cold molecular beam.[18] They assigned the fluorescence to a V→N emission, with a lifetime of 33 ± 5 ns at 231.5 nm excitation. The fluorescence quantum yield rapidly decreases at shorter wavelengths, explained as being due to an increased non-radiative decay rate. No fluorescence has been found from ethylene. In 2002, Rijkenberg *et al*. studied the resonance-enhanced multiphoton ionization (REMPI) spectra of jet-cooled tetramethylethylene.[19] The π3s Rydberg state was identified as the intermediate in the (1 + 1) REMPI excitation spectrum for a one-photon energy range of 415 00–440 00 cm^{-1} (241.0–227.2 nm). The observed rapid decrease in REMPI signal at shorter wavelengths was attributed to the internal conversion of the π3s Rydberg state to the $\pi\pi^*$ valence state.

The experimental and theoretical studies of excited state dynamics in ethylene and methyl substituted ethylenes have been mainly focused on the V state. There are a few studies of the Rydberg state dynamics, the subject of the present study. The dynamics of electronically excited ethylene and deuterated ethylene at 162 nm was interrogated in a previous study using an 11 fs pump laser pulse.[20] At this wavelength, absorption is dominated by the transition to the V state, with only small contributions from the π3s Rydberg state. It was suggested that the initially populated π3s Rydberg state appears to decay to the V state within 80 fs, whereupon it follows the canonical dynamics of the V state. The ultrafast dynamics of cyclohexene[8,21] and d_{10}-cyclohexene[21] excited at 200 nm was studied by fs time-resolved photoelectron spectroscopy[8] (TRPES) and by mass-selective strong field ionization.[21] The initially excited π3s Rydberg state appeared to decay to the V state within 20 fs. This rapidity was rationalized by claiming the small barrier encountered via passage around the lower cone of the 3s/$\pi\pi^*$ conical intersection would be easily surmounted. This mechanism was also used to explain the ultrafast decay of the 3*s* state of a few other systems.[22,23] The coupling of the V and Rydberg states has been discussed in a number of previous studies.[24–29] In the simulation of the ethylene absorption spectrum, Martinez and co-workers found that the coupling of the π3s Rydberg state with the V state had to been taken into account in order to reproduce the experimentally observed doublet-like structure.[29]

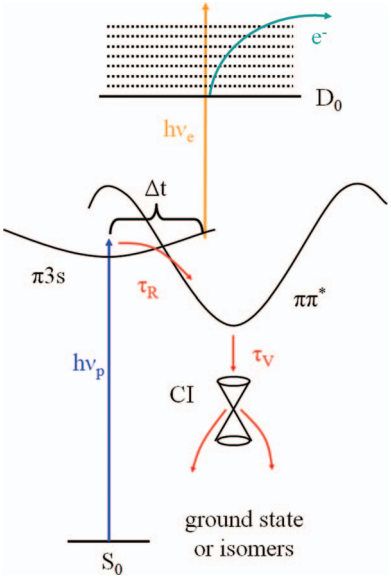

FIG. 1. The TRPES scheme and proposed picture for excited state dynamics of 1,2-dimethylethylene (*cis*-butene and *trans*-butene), trimethylethylene, and tetramethylethylene upon excitation of the π3s Rydberg state. The π3s state decays to the $\pi\pi^*$ state, the latter subsequently decaying to the ground state, presumably via an "ethylene-like" mechanism.

In the following, we describe the TRPES (Ref. 30) method used for the experimental study of π3s Rydberg state dynamics in isolated methyl ethylenes, shown schematically in Figure 1. Along with the experimental results, detailed *ab initio* calculations were performed in order to rationalize the observations. A detailed discussion of the effect of methyl substitution on the π3s Rydberg state dynamics ensues, followed by conclusions and prospects for future directions.

II. METHODS

A. Experimental method

We briefly describe our femtosecond time-resolved magnetic bottle photoelectron spectrometry method, detailed in Ref. 31. Due to the red-shifting of the UV absorption spectrum upon methylation, the fs pump laser wavelength was systematically tuned so as to maintain resonance with the π3s Rydberg state. For *cis*-butene and *trans*-butene, the pump wavelength was 200.5 nm, with a fs probe wavelength of 224.8 nm. For trimethylethylene, the fs pump and probe laser pulses were 215.9 nm and 266.5 nm, respectively. For tetramethylethylene, pump wavelengths of 215.9 nm, 219.3 nm, 222.4 nm, 224.5 nm, 229.2 nm, and 232.4 nm were used, all with a probe wavelength of 266.5 nm. Femtosecond laser pulses were obtained from a Ti:Sapphire regenerative amplifier (Coherent, Legend, 800 nm). Part of the output (∼700 μJ) was used for harmonic generation to produce 200.5 nm or 266.5 nm laser pulses. A second part (∼700 μJ) was used to pump a TOPAS (optical parametric amplifier, Light Conversion) system. The idler output from the TOPAS was doubled in a beta barium borate (BBO) crystal and summed with an external 800 nm pulse (∼460 μJ) in a second BBO crystal. The resulting sum frequency was then doubled in a third BBO crystal to generate fs UV laser pulses tunable between

TABLE I. 2D globally fitted time constants for *cis*-butene, *trans*-butene, trimethylethylene, and tetramethylethylene. τ_R and τ_V represent lifetimes of the $\pi 3$s Rydberg state and the $\pi\pi^*$ valence state, respectively, as detailed in the text. The pump and probe laser wavelengths (energies) used for each molecule and corresponding cross-correlations are also included.

	IP (eV)	Pump/probe (nm) (pump/probe (eV))	Cross-correlation (fs)	τ_R (fs)	τ_V (fs)
Cis-butene	9.11	200.5/224.8 (6.18/5.52)	122 ± 10	17 ± 10	38 ± 10
Trans-butene	9.10			19 ± 10	88 ± 10
Trimethylethylene	8.69	215.9/266.5 (5.74/4.65)	133 ± 10	23 ± 10	132 ± 10
Tetramethylethylene	8.27			5.6 ± 0.2 ps	
		219.3/266.5 (5.65/4.65)	135 ± 10	7.3 ± 0.1 ps	
		222.4/266.5 (5.57/4.65)	150 ± 10	8.1 ± 0.1 ps	
		224.5/266.5 (5.52/4.65)	140 ± 10	11.8 ± 0.1 ps	
		229.2/266.5 (5.41/4.65)	180 ± 10	14 ± 1 ps/72 ± 5 ps	
		232.4/266.5 (5.33/4.65)	225 ± 10	22 ± 2 ps /439 ± 14 ps	

215.9 nm and 232.4 nm. The fs UV pulses were individually recompressed using vacuum ultraviolet-grade CaF_2 prism pairs, combined collinearly on a dichroic mirror, and then gently focused using *f*/125 spherical reflective optics to intersect a seeded, pulsed molecular beam in the interaction region of a magnetic bottle photoelectron spectrometer. Time delays between pump and probe pulses were scanned using a computer-controlled stepper motor. Pulsed seeded (1%) supersonic molecular beams containing *cis*-butene (Aldrich, ≥99%), *trans*-butene (TCI America, ≥99%), trimethylethylene (Sigma-Aldrich, ≥99%), or tetramethylethylene (Sigma-Aldrich, ≥99%) in 3–4 bars helium carrier gas were generated using a 1 kHz Even-Lavie pulsed valve. Photoelectron spectra arising from the pump and probe laser pulses at negative time delays (i.e., the probe preceding the pump) were recorded and subtracted in order to correct for background photoelectrons generated from single laser multiphoton ionization.

Electron kinetic energy calibration was achieved using the well-characterized two-photon ionization of nitric oxide.[32,33] Time zero overlap and cross-correlations (i.e., instrumental response function) between the pump and the probe pulses were determined by $1+1'$ photoionization of nitric oxide or 1,3-butadiene. The cross-correlation data are included in Table I.

B. Computational methods

The potential energy surfaces of ethylene and the methylated ethylenes were investigated employing *ab initio* electronic structure methods. The vertical excitation energies, the global minima of the ground and the $\pi 3s$ Rydberg states, and the minimum energy conical intersections (MECI) between the $\pi 3s$ Rydberg and $\pi\pi^*$ valence states were optimized employing a 3s2p1d/2s1p atomic natural orbital (ANO) basis[34] set in conjunction with multi-reference configuration interaction with single and double excitations (MR-CISD) wavefunctions. The ANO basis was augmented with a pair of *s* and π diffuse functions, optimized from cationic energies and expanded in a basis of universal exponents,[35–37] centered at the ethylenic carbons of each molecule. The complete active space self-consistent field (CASSCF) optimized reference functions were computed using a (2,3) active space that corresponds to the π, π^*, and 3*s* orbitals. The **g** (energy difference gradient) and **h** (collinear with the non-adiabatic coupling gradient) (Ref. 38) directions associated with the $\pi 3$s/$\pi\pi^*$ MECIs were calculated for each molecule. These vectors, the Cartesian geometries of the ground and $\pi 3s$ Rydberg state minima, as well as the $\pi 3s$/ $\pi\pi^*$ MECI, are given as in supplementary material.[39] Furthermore, for tetramethylethylene, the harmonic frequencies at ground state, the $\pi 3s$ Rydberg state, and a constrained $\pi\pi^*$ valence state minimum were computed at the same level of theory and are also presented in the supplementary material. All electronic structure computations in this report were performed with the COLUMBUS suite of programs.[40,41]

C. Data analysis methods

A 2D global least-squares method was employed to fit all photoelectron kinetic energies and time delays simultaneously, using a Levenberg-Marquardt algorithm. For *cis*-butene, *trans*-butene, and trimethylethylene, it was found that the simplest model to non-trivially fit all measured transients was comprised of the cross-correlation plus two time constants. By contrast, for tetramethylethylene, it was found that the cross-correlation plus two or more time constants were required, depending on the pump laser wavelength. As a didactic example, the two-time-constant kinetic model which numerically simulates the 2D experimental data involves a convolution of the following expression:

$$\left.\begin{aligned} &\text{for } t \geq 0,\ S(\varepsilon_k, t) = D_A(\varepsilon_k)\exp\left(-\tfrac{t}{\tau_A}\right) + D_B(\varepsilon_k)\exp\left(-\tfrac{t}{\tau_B}\right), \\ &\text{for } t < 0,\ S(\varepsilon_k, t) = 0, \end{aligned}\right\} \tag{1}$$

with a Gaussian cross-correlation function which was determined separately. Here, ε_k is the kinetic energy of the emitted photoelectrons. The $D_A(\varepsilon_k)$ and $D_B(\varepsilon_k)$ are decay associated spectra (DAS), which are the energy-resolved amplitudes of components having time constants τ_A and τ_B, respectively. This expression can be used to represent two different kinetic models: a parallel or a sequential one. As discussed below, depending on the kinetic model, the DAS may or may not be directly proportional to the state-resolved photoelectron spectrum (i.e., energy-resolved photoionization cross section) $\sigma(\varepsilon_k)$. In a parallel model, the pump laser simultaneously prepares two excited states, *A* and *B*, which then

decay independently, each with its own lifetime of τ_A or τ_B. Here, $D(\varepsilon_k)$ equals the product of initial population n with the energy-resolved photoionization cross section $\sigma(\varepsilon_k)$ of the corresponding state having lifetime τ. In this case, the DAS are non-negative at all ε_k. By contrast, in a sequential model, an excited state A prepared by the pump pulse decays to state B with a time constant τ_A, which itself subsequently decays with time constant τ_B. The sequential model can be expressed in the form

$$\left.\begin{aligned} &\text{for } t \geq 0,\ S(\varepsilon_k, t) = n\sigma_A(\varepsilon_k)\exp\left(-\tfrac{t}{\tau_A}\right) + n\tfrac{\tau_B}{\tau_B-\tau_A}\sigma_B(\varepsilon_k) \\ &\qquad\qquad \times\left[\exp\left(-\tfrac{t}{\tau_B}\right) - \exp\left(-\tfrac{t}{\tau_A}\right)\right], \\ &\text{for } t < 0,\ S(\varepsilon_k, t) = 0. \end{aligned}\right\} \quad (2)$$

As in the parallel model, $\sigma_A(\varepsilon_k)$ and $\sigma_B(\varepsilon_k)$ represent the energy-resolved photoionization cross sections of states A and B, respectively, and n is the initial population on state A. In this case, the DAS of τ_A is

$$D_A(\varepsilon_k) = n\left[\sigma_A(\varepsilon_k) - \frac{\tau_B}{\tau_B - \tau_A}\sigma_B(\varepsilon_k)\right], \quad (3)$$

which, we note, can be negative at certain kinetic energies ε_k, depending on the relative magnitudes of the energy-resolved photoionization cross sections of states A and B. Indeed, negative amplitudes are indicative of a sequential model. The DAS for time constant τ_B is

$$D_B(\varepsilon_k) = n\frac{\tau_B}{\tau_B - \tau_A}\sigma_B(\varepsilon_k), \quad (4)$$

which is proportional to the energy-resolved photoionization cross section of state B.

III. RESULTS

A. Experimental results

The TRPES spectra for *cis*- and *trans*-butene excited at 200.5 nm, trimethylethylene at 215.9 nm, and tetramethylethylene at 232.4 nm are shown in Figures 2–5. For each molecule, the DAS extracted from the fit are presented beneath the corresponding TRPES data. The time constants derived from the fit for *cis*-butene, *trans*-butene, and trimethylethylene and time constants assigned to the π3s Rydberg state for tetramethylethylene (see the assignment in Sec. IV A) are given in Table I. The error bars are based on the uncertainties in the time zeros, the cross correlations, and statistical errors in the data. The origin and physical interpretation of these time constants will be discussed in Sec. IV A.

B. Theoretical results

In Figure 6(a), we show the vertical excitation energies for each of ethylene (C_2H_4), propene (C_3H_6), *cis*-butene and *trans*-butene (C_4H_8), trimethylethylene (C_5H_{10}), and tetramethylethylene (C_6H_{12}). While experimental data for the first two species were not recorded, they are included in the computational results for a clearer presentation of the trends in the series. These values appear to overestimate the excitation energies (particularly for the valence states), but the trends are

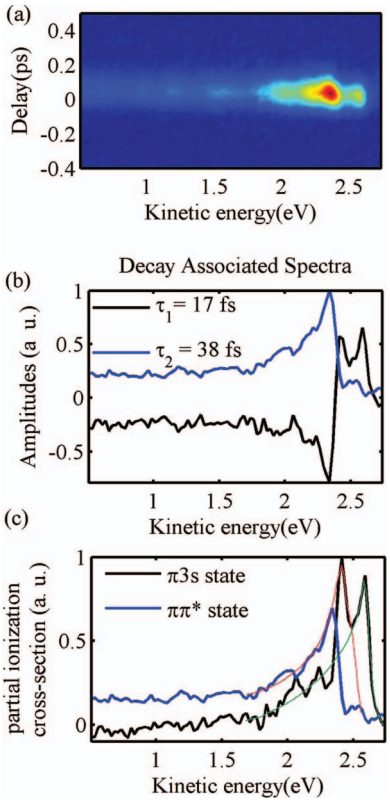

FIG. 2. (a) TRPES spectrum of *cis*-butene at pump and probe wavelengths of 200.5 nm and 224.8 nm, respectively. (b) Decay associated spectra (DAS) associated with the two time constants derived from a 2D global least-squares fit. (c) Photoionization cross sections derived from the DAS by assuming initial excitation to the π3s Rydberg state alone. The relationship between partial photoionization cross sections and decay associated spectra as discussed in Sec. II C. Due to the proximity of the two time constants (17 and 38 fs), the global fitting routine does not fully separate these two spectra. The thin red line indicates the expected photoelectron spectrum of the $\pi\pi^*$ state whereas the thin green line indicates the same for the π3s state.

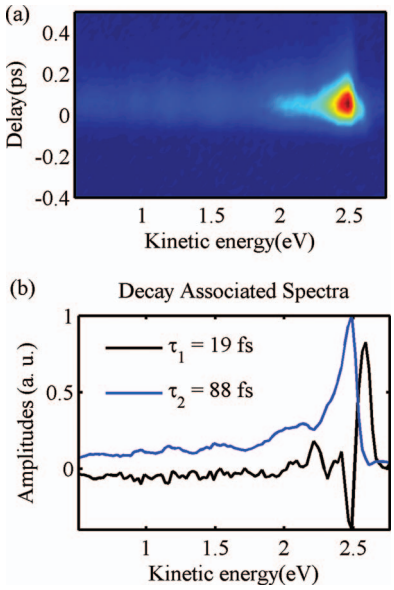

FIG. 3. (a) TRPES spectrum of *trans*-butene at pump and probe wavelengths of 200.5 nm and 224.8 nm, respectively. (b) Decay associated spectra (DAS) associated with the two time constants derived from a 2D global least-squares fit.

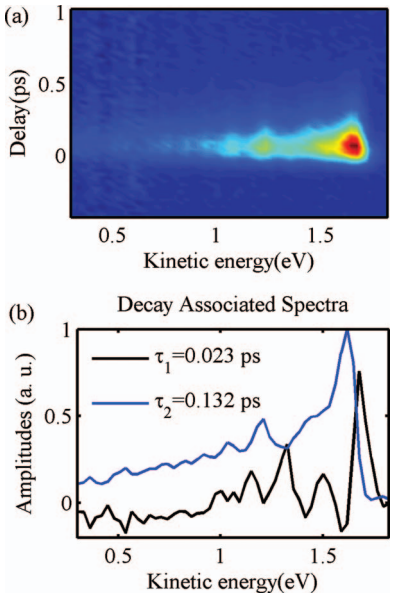

FIG. 4. (a) TRPES spectrum of trimethylethylene at pump and probe wavelengths of 215.9 nm and 266.5 nm, respectively. (b) Decay associated spectra (DAS) associated with the two time constants derived from a 2D global least-squares fit.

clear: while the vertical excitation energy to the lowest valence state decreases (unevenly) by ∼0.3 eV on going from ethylene to tetramethylethylene, the excitation energy to the $\pi 3s$ Rydberg state decreases rapidly and monotonically by ∼1.5 eV, from 7.1 to 5.6 eV. The observation which hints at a unified perspective on these excited state dynamics is that as methyl groups are added to the ethylenic moiety, the vertical excitation energy of the low-lying Rydberg state decreases more rapidly than that of the valence state.

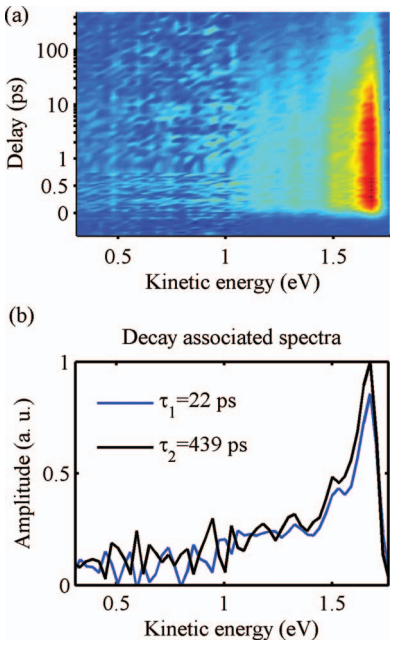

FIG. 5. (a) TRPES spectrum of tetramethylethylene at pump and probe wavelengths of 232.4 nm and 266.5 nm, respectively. Note that a combination of linear and logarithmic scales is used in the ordinate. (b) Decay associated spectra (DAS) associated with the two time constants derived from a 2D global least-squares fit.

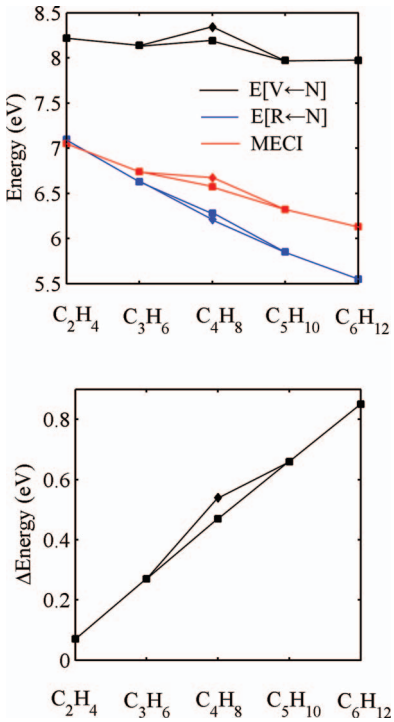

FIG. 6. (a) Vertical excitation energies to the $\pi 3s$ Rydberg and $\pi\pi^*$ states, and energy of the $\pi 3s/\pi\pi^*$ MECI, for each member of the series ethylene (C_2H_4), methylethylene (propylene, C_3H_6), 1,2-dimethylethylene (C_4H_8), trimethylethylene (C_5H_{10}), and tetramethylethylene (C_6H_{12}). For C_4H_8, there exist two isomers, *cis*-butene and *trans*-butene, denoted by (♦) and (■), respectively. (b) Energy differences between the optimized minimum of the $\pi 3s$ Rydberg state and the $\pi 3s/\pi\pi^*$ MECI.

The energy of the $\pi 3s/\pi\pi^*$ MECI for each member of the series is also shown in Figure 6(a). While there may be systematic overestimation of the energy of the MECI relative to the Rydberg minimum, the trend is clear: the energy of the $\pi 3s/\pi\pi^*$ MECI monotonically decreases with the increasing substitution. In order to more clearly elucidate the consequences of the increasing energy gap between the $\pi 3s$ and $\pi\pi^*$ excited states, Figure 6(b) evinces the energy difference between the $\pi 3s$ Rydberg minimum and the corresponding $\pi 3s/\pi\pi^*$ MECI for each member of the series. As clearly shown by the plot, this energy difference increases upon increasing substitution, from 0.05 eV in ethylene to almost 0.9 eV in tetramethylethylene.

While the optimized Cartesian geometry of each MECI in given in Tables S1–S6 in the supplemental material,[39] the largest amplitude displacement from the FC geometry to the intersection is described by the torsion angle, θ_{MECI}, about the ethylenic carbon-carbon bond. This angle is defined as the average of the four dihedral angles, where the planar configuration is defined to have a value of zero. The value of this angle is presented in Table II for each member of the series. As the energy difference between these two states grows, the torsional displacement required to obtain degeneracy between the valence and Rydberg states displays a concomitant increase, moving the intersection point further from the FC

TABLE II. Computed energy differences between the $\pi 3s/\pi\pi^*$ MECI and the $\pi 3s$ Franck-Condon geometry as well as the corresponding torsional angle for each. Both the energy difference and MECI torsional angle increase upon methylation.

	E_{MECI}–E_{FC} (eV)	θ_{FC} (°)	θ_{MECI} (°)
Ethylene	−0.05	0.0	33.2
Propene	0.11	0.0	39.8
Trans-butene	0.29	0.0	47.4
Cis-butene	0.46	0.0	46.8
Trimethylethylene	0.47	0.0	57.5
Tetramethylethylene	0.58	3.7	62.8

window. Furthermore, as the first column of Table II shows, with the exception of ethylene for which the energy of $\pi 3s/\pi\pi^*$ MECI lies below the energy of the FC point, there is a small but increasing barrier to the MECI upon methylation. In fact, for tetramethylethylene, this barrier (the difference in energy between the $\pi 3s/\pi\pi^*$ MECI and $\pi 3s$ Rydberg state at the FC geometry) has increased to almost 0.6 eV. Therefore, in tetramethylethylene, unless the excited state wavepacket is prepared with a significant amount of internal energy, accessing the MECI may be difficult.

The two directions along which the degeneracy is broken at first order, **g** and **h**, were also calculated at the $\pi 3s/\pi\pi^*$ MECI for each member of this series, as shown in Figure S1 of the supplemental material.[39] The **g** vectors are predominantly torsion about the central C–C bond but also involve significant central C–C stretch. The **h** vectors are somewhat more complicated (particularly for the lower symmetry species), but show systematic changes upon substitution. In ethylene, the **h** direction is characterized by the asymmetric C–H stretch. Upon methylation, the torsional angles at the MECI increase, and these vectors rotate "out of the plane" until this direction is predominantly pyramidalization at the central C–C carbons for tetramethylethylene.

In order to assess the relevance of CI mediated dynamics to the excited state lifetime of tetramethylethylene, we performed model computations of the rate of radiationless transitions from the $\pi 3s$ Rydberg state into the manifold of $\pi\pi^*$ vibronic states. Within the model, the rate of internal conversion is proportional to the sum of the squares of the non-adiabatic coupling matrix elements and is computed according to the expression:

$$K = \frac{2\pi}{\hbar}\sum_f \left|\langle \Psi_f(\mathbf{r},\mathbf{Q})\,|-\sum_j^{N^{vib}}\frac{1}{2}\frac{\partial^2}{\partial Q_j^2}|\,\Psi_i(\mathbf{r},\mathbf{Q})\rangle\right|^2 \times e^{-[(E_f-E_i)/\sigma]^2}, \quad (5)$$

where the number of internal nuclear degrees of freedom is given by $N^{vib} = 3N^{\text{atoms}} - 6$, **Q** and **r** are (mass-weighted, i.e., normal) the nuclear and electronic coordinates, respectively, E_f and E_i are the energies of the states ψ_f and ψ_i, and σ is a parameter that defines the energetic width of the wavepacket in the excited state manifold. For the following simulations, σ was set to 200 cm^{-1} in order to approximate the bandwidth of the pump pulse used in experiments. Taking the total wavefunction to be a product of electronic and nuclear functions,

$$\Psi(\mathbf{r},\mathbf{Q}) = \psi^e(\mathbf{r};\mathbf{Q})\prod_{m=1}^{N^{nvib}}\chi_m^e(Q_m), \quad (6)$$

where the superscript e = R or V, denoting the $\pi 3s$ Rydberg or $\pi\pi^*$ valence electronic states, respectively. Neglecting the second-derivative coupling contributions to the matrix element, this expression is expanded to give

$$K = \frac{-\pi}{\hbar}\sum_f \left|\sum_j^{N^{vib}}\langle\psi_f(\mathbf{r};\mathbf{Q})|\frac{\partial}{\partial Q_j}|\,\psi_i(\mathbf{r};\mathbf{Q})\rangle \times \langle\chi_f(\mathbf{Q})|\frac{\partial}{\partial Q_j}|\,\chi_i(\mathbf{Q})\rangle\right|^2 e^{-[(E_f-E_i)/\sigma]^2}. \quad (7)$$

The integral over the electronic component of the wavefunction is obtained from *ab initio* computations,[42,43] while the integral over the nuclear functions may be readily determined from Franck-Condon integrals if a harmonic oscillator basis is employed.[44–46]

In the following analysis, the large amplitude torsional mode, characterized by the dihedral angle (θ) about the C–C bond, will be treated separately from the remaining $N^{vib}-1$ normal coordinates, such that $\mathbf{Q} = \{\mathbf{q},\theta\}$. Therefore, the initial and final state wavefunctions denoted in Eq. (6) may be re-expressed as

$$\Psi_n^e(\mathbf{q},\theta,\mathbf{r}) = \psi^e(\mathbf{r};\mathbf{q},\theta)\chi_{n,\theta}^e(\theta)\prod_{m=1}^{N^{vib}-1}\chi_{n,m}^e(q_m)m, \quad (8)$$

where the $\chi_{n,m}^e(q_m)$ are harmonic oscillator basis functions for the normal modes, the $\chi_{n,\theta}^e(\theta)$ are the basis functions which characterize the dihedral angle (θ) coordinate, and are obtained as the solutions of the following equations:

$$\left[-\frac{a^e}{2I^e}\frac{\partial^2}{\partial\theta^2} + \frac{1}{2}\begin{pmatrix} U_1^e(1-\cos[2(\theta-\theta_0)])+ \\ U_2^e(1-\cos[4(\theta-\theta_0)])\end{pmatrix} - (E_n^e - E_0^e)\right]\chi_{n,\theta}^e(\theta) = 0. \quad (9)$$

The values of the parameters U_1^e and U_2^e were determined from a least-squares fit of *ab initio* energies at six equidistant points along the torsional coordinate from 0° to 90° (as well as $\theta = 6.9°$ for the 3*s* Rydberg state). The I^e are the moments of inertia about the C–C bond (computed from the optimized geometries), and the parameters a^e are employed as scale factors to ensure that the analytic potentials approximately reproduce the torsional mode *ab initio* fundamentals within each state, given by 101 cm^{-1} and 369 cm^{-1} for the $\pi 3s$ and $\pi\pi^*$ states, respectively. The application of these constraints, and the expansion of the $\chi_{n,\theta}^e(\theta)$ in a Fourier series basis, yielded the following parameters (in a.u. unless specified): (a^e, I^e, U_1^e, U_2^e, θ_0^e, E_0^e) = (10, 759 659, 0.049 30, −0.015 49, 6.9°, 0) and (10, 802 160, −0.074 02, −0.001 94, 0°, 0.067 220 1)

TABLE III. Computed tetramethylethylene $\pi 3s$ Rydberg state lifetimes for radiationless transitions to the valence $\pi\pi^*$ electronic state, as a function of the number of quanta v_θ in the C–C double bond torsional mode. For a description of the radiationless transition model, see Sec. III B.

v_θ	$E_{v_\theta}^{3s}$ (cm^{-1})	τ (ps)
0	0	42843
1	101	5628
2	223	569
3	377	71
4	550	14

for e = R and V, respectively. The potential function for the V state yields doubly degenerate torsional levels (E_1 = 281 cm^{-1}), while the Rydberg state potential function yields pairs of doubly degenerate energy levels (E_1 = 101 cm^{-1}) which were energy-averaged to yield quasi-quadruply degenerate levels (thereby reducing the number of Franck-Condon type integrals requiring computation). The above parameters result in a crossing between the two curves at a dihedral angle of 60° and at an energy of 0.48 eV above the Rydberg state FC point: this reasonably approximates the *ab initio* potential data given in Table II and Fig. 6. Note that this approach is completely analogous to that of Zerbetto and Zgierski,[47] who employed a similar ansatz to study the rate of radiationless transitions between the 2^1A_g and 1^1A_g states of butadiene. That study determined that the rate of transitions between the excited and ground electronic states was profoundly sensitive to the dihedral angle about the terminal C–C bond, increasing by orders of magnitude as this angle was increased away from the planar ground state equilibrium geometry.

Converged transition rates were obtained by evaluating all non-adiabatic matrix elements involving up to five quanta in a given vibrational coordinate, except for the torsional coordinate upon which no excitation restrictions were placed. This is the so-called "accepting" mode in the nomenclature of Siebrand and Zgierski.[48,49] The results of these calculations are given in Table III. While the absolute value of the computed lifetime for the lowest vibrational level of the $\pi 3s$ Rydberg state is significantly longer (43 ns) than the longest time constant extracted from the TRPES data (439 ps), the computed lifetimes display a pronounced dependence on the excitation level of the torsional mode, decreasing roughly by an order of magnitude upon each successive excitation. This trend was computed up to v = 4, which corresponds to an energy only 550 cm^{-1} above the v = 0 torsional level, but results in a lifetime of only 14 ps–a difference of more than 3 orders of magnitude. This level is in better accord with the second time constant determined from the experimental measurements (22 ps). Given the large error bars that would be expected for this relatively qualitative computation, an attempt to make a direct assignment of the vibrational states involved would be ill-advised. Rather, the utility of these computations is found in the validation of the proposed non-radiative decay channel, as well as the vibrational state dependence of the excited state lifetime, which will be discussed in more detail below.

IV. DISCUSSION

A. Assignment of the fitted time constants

It is always possible to trivially improve a fit by adding more components to the fitting procedure. The reduced χ^2 is a statistical measure used to determine if an additional fit component is non-trivially required. However, in our situation, providing TRPES spectral evidence (i.e., comparing the forms of the DAS) is the most physically intuitive justification. In other words, the form of the energy-resolved photoelectron spectra can help with the assignment of channels as being of Rydberg or valence character. In the following, we discuss the assignment of the time constants derived from our 2D fits.

For *cis*- and *trans*-butene at 200.4 nm and trimethylethylene at 215.9 nm, both the $\pi\pi^*$ valence and $\pi 3s$ Rydberg states could conceivably be excited. Normally, a strongly allowed $\pi\pi^*$ valence state should dominate the photoabsorption. However, due to its twisted geometry, it is greatly disfavored (at the given pump wavelengths) due to its small FC factors, thus potentially rendering both states operational. This might suggest initial use of a parallel kinetic model. We anticipate, however, that any direct excitation of the $\pi\pi^*$ state would lead to "ethylene-like" ultrafast monoexponential decay.[20,50–53] In our biexponential fitting procedure, an ultrafast $\pi\pi^*$ parallel decay channel would contribute only to the fastest component which has amplitude near $\Delta t = 0$. We note that (i) the relative contribution (at 200 nm) of the $\pi\pi^*$ state is unknown, and (ii) we have clear evidence for a sequential process, indicating that any parallel $\pi\pi^*$ channel contribution must be small, which is consistent with the absorption spectra. Therefore, we will model the dynamics as a sequential process involving direct preparation of the $\pi 3s$ Rydberg state alone, followed by its sequential decay to the $\pi\pi^*$ state. Nevertheless, it must be understood in the following that the fastest time constant and the form of its correlated DAS potentially contain unresolved minor contributions from an ultrafast $\pi\pi^*$ parallel decay channel.

For *cis*-butene at 200 nm, Fig. 2, the DAS associated with the 38 fs time constant has positive value over the whole spectrum, while that of the 17 fs time constant has negative values over a broad range of electron kinetic energies. Therefore, the 17 fs constant is assigned to the lifetime of the $\pi 3s$ Rydberg, the first step in a sequential process. Making use of our calculations (see Table II, Fig. 6, and supplemental material)[39] and analogies between ethylene and methyl substituted ethylenes, we believe that the $\pi 3s$ Rydberg state is crossed by the $\pi\pi^*$ state at a twisted geometry. Therefore, the second state in the sequential model should be the $\pi\pi^*$ state, which itself subsequently decays to the ground state, presumably via "ethylene-like" dynamics, in 38 fs. The partial photoionization cross sections (i.e., the photoelectron spectra) derived from the DASs (see Sec. II C) are shown in Fig. 2(c). The argumentation for *trans*-butene and trimethylethylene proceeds in an analogous manner. Since the two time constants for *cis*-butene are within the same decade, it is difficult to fully separate the two-photoelectron spectra. Due to this, the numerically extracted photoelectron spectra, shown

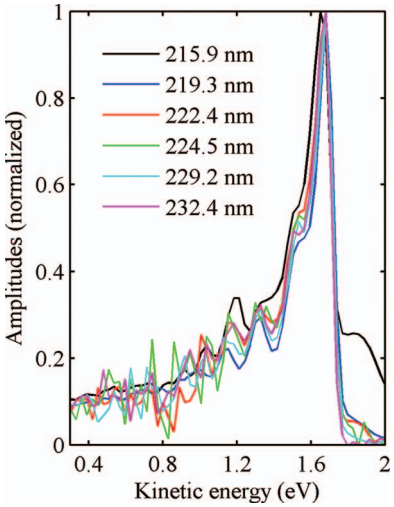

FIG. 7. Tetramethylethylene decay associated spectra (DAS) of the $\pi 3s$ Rydberg state as a function of wavelength between 215.9 nm and 232.4 nm. At 229.2 and 232.4 nm, there are two time constants assigned to the $\pi 3s$ Rydberg state, each having very similar DAS: only one is shown here for clarity, that with the smaller time constant.

as the blue line for the $\pi\pi^*$ state and the black line for the $\pi 3s$ state, show some mixing. For example, the photoelectron spectrum of the $\pi 3s$ state is not expected to show a double peak structure at its origin. For this reason, we have sketched, in green for the $\pi 3s$ and in red for the $\pi\pi^*$ states, the expected forms of the photoelectron spectrum associated with each state, as a guide to the eye. It is conceivable that more sophisticated global fitting methods may improve the numerical separation of these associated photoelectron spectra.

In order to fit the tetramethylethylene data, we started with the longest wavelength, 232.4 nm, where photoabsorption is to the $\pi 3s$ Rydberg state alone. Two time constants were extracted and the DASs, neither having negative amplitude at any electron kinetic energies, support a parallel kinetic model. These two photoelectron spectra (equivalent to the DASs in a parallel model, as discussed in Sec. II C) are very similar, both dominated by a single strong peak at the same energetic position. These spectra, showing a limited Franck-Condon progression, are consistent with the photoionization of a Rydberg state. At shorter wavelengths, we found components (two at 229.2 nm, one at the other wavelengths) having similar Rydberg-like DAS and associated time constants of similar order of magnitude, the comparison being given in Fig. 7. The DAS again have a single strong peak at the same energetic position, despite the energy difference between 215.9 nm and 232.4 nm being ~0.4 eV. The pump energy independence of this photoelectron spectrum and its single intense peak are strong indications of the photoionization of a Rydberg state. In Ref. 19, the (1+1) REMPI photoelectron spectrum of tetramethylethylene at one-photon energy of 42842 cm^{-1} (233.4 nm) was reported and the $\pi 3s$ Rydberg state was identified as being the resonant state. Significant similarities are observed between this previous study and our energy-resolved photoelectron spectra. Therefore, these observations lead to an assignment of this component to the $\pi 3s$ Rydberg state. Furthermore, at 229.2 nm and 232.4 nm, the absorption spectrum of tetramethylethylene is dominated by transition to the $\pi 3s$ Rydberg state. We note that no other state has been reported in the same energy region. Therefore, the second component is tentatively assigned to the $\pi 3s$ Rydberg state as well. The possible reasons that there are two components having different lifetimes, yet associated with the Rydberg state, will be discussed in later section.

In summary, 200.5 nm excitation of *cis*-butene and *trans*-butene, or 215.9 nm excitation of trimethylethylene populates mainly the $\pi 3s$ Rydberg state, which subsequently decays to the $\pi\pi^*$ state (and finally to the ground state), as depicted in Fig. 1. For the case of tetramethylethylene at 229.2 nm and 232.4 nm, absorption is only to the $\pi 3s$ Rydberg state, which at these energies persists 3 to 4 orders of magnitude longer than that of the dimethyl and trimethyl species. With increasing excitation energy, the decay rate of the tetramethylethylene $\pi 3s$ Rydberg state increases, but at a much slower rate than those of the dimethyl and trimethyl species. In Table I, we present the fitted time constants for all molecules, labeled as τ_R and τ_V, which correspond to the lifetime of the $\pi 3s$ Rydberg state and the $\pi\pi^*$ state, respectively.

B. Non-radiative decay processes

The $\pi 3s$ Rydberg state lifetimes of *cis*-butene, *trans*-butene, and tetramethylethylene are in reasonably good agreement with those derived from fluorescence quantum yield measurements.[16] The lifetimes of tetramethylethylene derived from other fluorescence studies are much longer: 20.8 ± 0.9 ns at 235 nm (Ref. 17) or 33 ± 5 ns at 231.5 nm.[18] The monotonic decrease in lifetime of the tetramethylethylene $\pi 3s$ Rydberg state observed in our measurements is consistent with the observations in the fluorescence studies: the fluorescence yield rapidly decreases at shorter wavelengths.[18]

The extremely short Rydberg state lifetimes of *cis*-butene and *trans*-butene at 200 nm and trimethylethylene at 215.9 nm are not unprecedented and have been observed in other unsaturated hydrocarbons such as cyclopentadienes[6,7] and cyclohexenes.[8,21] The rationale is that these Rydberg states often possess some degree of valence character[10,14] and the low lying $n = 3$ member would be expected to be strongly coupled to the valence manifold.

Ab initio computations (Fig. 6 and Table II) show that although energy difference between the $\pi 3s$ Franck-Condon region and the $\pi 3s/\pi\pi^*$ MECI increases upon methylation, it nevertheless remains small in absolute magnitude for *cis*-butene, *trans*-butene and, arguably, trimethylethylene. The predominant geometrical distortion leading to these MECIs is torsion about the central C–C double bond. We further note that species having a larger energy difference achieve the MECI at an increased torsional angle. Thus, upon methylation, the $\pi 3s/\pi\pi^*$ MECI occurs not only at relatively higher energy, but correspondingly at geometries further displaced from the FC point. The extremely short Rydberg state lifetimes for the dimethyl and trimethyl species suggest that the initially prepared wavepackets on the $\pi 3s$ Rydberg surfaces rapidly access the coupling region associated with the $\pi 3s/\pi\pi^*$ MECI. This implies, for dimethyl- and trimethylethylene, that any energetic barriers to the MECI

region are easily surmounted. Following transition to the $\pi\pi^*$ valence state, we assume that the dynamics follow the well-known intersection mediated pathways back to the ground electronic state. This mechanism has been used to explain the ultrafast decay of the $\pi 3s$ Rydberg state of cyclohexene and other molecules.[21–23]

In tetramethylethylene, the $\pi 3s$ decay rate at the longest wavelength (232.4 nm) is much slower than in dimethyl- and trimethylethylene. *Ab initio* computation shows that there is likely an increased energy barrier to accessing the $\pi 3s/\pi\pi^*$ MECI region and, therefore—the fast channel through CI region being closed—leads to a much slower decay. However, the dependence of the $\pi 3s$ Rydberg state lifetime on the excitation energy seems to indicate that there may be other factors at play. At 215.9 nm, the $\pi 3s$ Rydberg state of trimethylethylene has an ultrashort lifetime (23 fs), while that of tetramethylethylene is more than 100 times longer (5.6 ps). The ultrafast decay of trimethylethylene suggests that, at this pump laser wavelength, the wavepacket should have sufficient internal energy to overcome the small barrier to the $\pi 3s/\pi\pi^*$ MECI region. However, according to our calculations (Fig. 6), the $\pi 3s/\pi\pi^*$ MECI of tetramethylethylene is energetically below that of trimethylethylene and, therefore (at 215.9 nm), tetramethylethylene should also readily access the $\pi 3s/\pi\pi^*$ MECI region and exhibit ultrafast decay. This is contrary to what was observed. Therefore, we suggest that for tetramethylethylene, the following two factors may also play important roles: (1) the larger torsional displacement of the $\pi 3s/\pi\pi^*$ MECI from the $\pi 3s$ Franck-Condon region may make accessing this CI region more difficult, and (2) the **h** vector is dominated by pyramidalization at the ethylenic C–C carbons. Displacement along the pyramidalization coordinate (which lower the barrier from the $\pi 3s$ Rydberg to the $\pi\pi^*$ state) would presumably be subject to steric effects, given the comparatively bulky methyl groups, and may inhibit the "skirting" of wavepacket around the lower cone of CI. These two effects dramatically reduce the decay rate to the V state. In this situation, a description of the decay mechanism via CI may not be appropriate. In tetramethylethylene, we believe, based on our calculations, that the predominant decay channel is still to the valence $\pi\pi^*$ state (analogous with the other members of the series). However, given the barriers and larger displacement to accessing the MECI, the role of CI in tetramethylethylene is significantly diminished. The computations presented in Sec. III B present an alternate $\pi 3s$ decay mechanism for tetramethylethylene. Even in the absence of a CI, the $\pi 3s$ Rydberg state contains significant valence character, resulting in rates of internal conversion that are competitive with fluorescence.

Finally, our computations show that the additional time constant observed in the decay of the $\pi 3s$ state of tetramethylethylene at the two longest pump wavelengths is most likely due to vibrational hot bands from the ground state. This suggests the incoherent decay of two independently prepared vibrational states in the 3*s* Rydberg electronic state, probably corresponding to the C–C twisting vibrational mode. Given that the *ab initio* computed harmonic fundamental for the ground state torsion is only 163 cm^{-1}, it is likely that the relatively inefficient cooling of thermal vibrational excitations in supersonic molecular beams could give rise to non-negligible population of these low-lying vibrational states. Due to possibly enhanced Franck-Condon factors for twisted ground state geometries, even small populations of vibrationally excited torsional modes may contribute comparably to the excited state population. Since there is no phase relationship between them, each ground vibrational state will produce an independent excited state wavepacket. This interpretation is consistent with both the trends and absolute values of the lifetimes shown in Table III. At the longest wavelengths where two time constants are required, the small but excess ground state vibrational energy due to the hot band transition has an observable effect. At shorter wavelengths, this small amount of ground state vibrational energy becomes relatively less important, and therefore a single time constant suffices. Experiments with elevated vibrational temperatures may help to validate this proposed mechanism.

V. CONCLUSIONS

Using a combination of TRPES and high-level *ab initio* calculations, we studied the $\pi 3s$ Rydberg state dynamics of 1,2-dimethylethylene (*cis*-butene and *trans*-butene), trimethylethylene, and tetramethylethylene. The 1,2-di- and tri-methyl substituted ethylenes exhibit ultrafast decay (~20 fs) to the $\pi\pi^*$ state, whereas that of the fully methylated ethylene is 2 to 4 orders of magnitude slower, depending on the excitation energy. These observations are rationalized by our calculations. The energetic barrier between the Franck-Condon region of the $\pi 3s$ Rydberg state and the $\pi 3s/\pi\pi^*$ MECI increases systematically upon methylation. Furthermore, upon increasing methylation, the geometry of the $\pi 3s/\pi\pi^*$ MECI systematically displaces along the torsional coordinate leading from the $\pi 3s$ Rydberg state. In tetramethylethylene, excitation to the $\pi 3s$ Rydberg state between 215.9 nm and 232.4 nm leads to a situation where the energetic barrier and geometric displacement required to access the $\pi 3s/\pi\pi^*$ MECI make the decay through CI very unlikely, significantly slowing down the decay rate.

Our proposed picture for the $\pi 3s$ Rydberg state dynamics and the dramatic changes in lifetime of the $\pi 3s$ Rydberg state from trimethylethylene to tetramethylethylene deserves more experimental and theoretical study. Time-resolved studies with even shorter pump and probe laser pulses will be helpful in more accurately determining the lifetimes of 1,2-dimethylethylene and trimethylethylene. Molecular frame time-resolved photoelectron angular distributions[54] may also provide additional views of the evolving electronic character of the excited states involved. We anticipate that the pump wavelength dependence of the $\pi 3s$ dynamics for 1,2-di- and tri-methyl substituted ethylenes will be very interesting, especially around the barrier region.

Finally, we note that methyl substitution in ethylene also affects the dynamics of the $\pi\pi^*$ valence state. Methylation affects the topography of the potential energy surfaces, the locations and shapes of the relevant CIs, the potential closure of the H-migration channel, the relative frequencies of key vibrational modes (e.g., torsion), etc. We will report on our TRPES

and *ab initio* studies of substitution effects on ethylene $\pi\pi^*$ state dynamics in a forthcoming paper.

ACKNOWLEDGMENTS

We thank NSERC for funding support. The authors thank M. Zgierski for insightful discussion. M.S. thanks S. Patchkovskii for assistance in the non-radiative decay rate computations. A.E.B. thanks the Swiss NSF (project No. PBBS2-115105), and O.S. thanks the Alexander von Humboldt Foundation for financial support.

[1] A. Stolow, B. A. Balko, E. F. Cromwell, J-S. Zhang, and Y. T. Lee, J. Photochem. Photobiol. A: Chem. **62**, 285 (1992).
[2] J. Quenneville and T. J. Martinez, J. Phys. Chem. A **107**, 829 (2003).
[3] A. Toniolo, B. Levine, A. Thompson, J. Quenneville, M. Ben-Nun, J. Owens, S. Olsen, L. Manohar, and T. J. Martinez, *Computational Methods in Photochemistry* (CRC, Boca Raton, 2004), pp. 167–234.
[4] B. G. Levine and T. J. Martinez, Annu. Rev. Phys. Chem. **58**, 613 (2007).
[5] B. G. Levine and T. J. Martinez, J. Phys. Chem. A **113**, 12815 (2009).
[6] W. Fuss, W. E. Schmid, and S. A. Trushin, Chem. Phys. **316**, 225 (2005).
[7] O. Schalk, A. E. Boguslavskiy, and A. Stolow, J. Phys. Chem. A **114**, 4058 (2010).
[8] O. Schalk, A. E. Boguslavskiy, A. Stolow, and M. S. Schuurman, "Through-bond interactions and the localization of excited-state dynamics," J. Am. Chem. Soc. (in press).
[9] P. G. Wilkinson and R. S. Mulliken, J. Chem. Phys. **23**, 1895 (1955).
[10] A. J. Merer and R. S. Mulliken, Chem. Rev. **69**, 639 (1969).
[11] M. B. Robin, *Higher Excited States of Polyatomic Molecules* (Academic, New York, 1975), vol. 2.
[12] M. B. Robin, *Higher Excited States of Polyatomic Molecules* (Academic, New York, 1985), vol. 3.
[13] F. H. Watson, Jr., A. T. Armstrong, and S. P. McGlynn, Theor. Chim. Acta **16**, 75 (1970).
[14] F. H. Watson, Jr. and S. P. McGlynn, Theor. Chim. Acta **21**, 309 (1971).
[15] H. Reisler and A. I. Krylov, Int. Rev. Phys. Chem. **28**, 267 (2009).
[16] F. Hirayama and S. Lipsky, J. Chem. Phys. **62**, 576 (1975).
[17] M. A. Wickramaaratchi, J. M. Preses, and R. E. Weston, Jr., Chem. Phys. Lett. **120**, 491 (1985).
[18] W. Siebrand, C. Dedonder-Lardeux, and C. Jouvet, Chem. Phys. Lett. **174**, 558 (1990).
[19] R. A. Rijkenberg, W. J. Buma, C. A. van Walree, and L. W. Jenneskens, J. Phys. Chem. A **106**, 5249 (2002).
[20] K. Kosma, S. A. Trushin, W. Fuss, and W. E. Schmid, J. Phys. Chem. A **112**, 7514 (2008).
[21] W. Fuss, W. E. Schmid, and S. A. Trushin, J. Am. Chem. Soc. **123**, 7101 (2001).
[22] W. Fuss, K. K. Pushpa, W. E. Schmid, and S. A. Trushin, J. Phys. Chem. A **105**, 10640 (2001).
[23] S. A. Trushin, S. Sorgues, W. Fuss, and W. E. Schmid, Chem. Phys. Chem. **5**, 1389 (2004).
[24] R. J. Buenker, S. D. Peyerimhoff, and H. L. Hsu, Chem. Phys. Lett. **11**, 65 (1971).
[25] L. E. McMurchie and E. R. Davidson, J. Chem. Phys. **66**, 2959 (1977).
[26] C. Petrongolo, R. J. Buenker, and S. D. Peyerimhoff, J. Chem. Phys. **76**, 3655 (1982).
[27] E. R. Davidson, J. Phys. Chem. **100**, 6161 (1996).
[28] T. Muller, M. Dallos, and H. Lischka, J. Chem. Phys. **110**, 7176 (1999).
[29] H. Choi, K. K. Baeck, and T. J. Martinez, Chem. Phys. Lett. **398**, 407 (2004).
[30] A. Stolow and J. G. Underwood, Adv. Chem. Phys. **139**, 497 (2008).
[31] S. Lochbrunner, J. Larsen, J. Shaffer, M. Schmitt, T. Schultz, J. Underwood, and A. Stolow, J. Electron Spectrosc. Relat. Phenom. **112**, 183 (2000).
[32] G. W. Bethke, J. Chem. Phys. **31**, 662 (1959).
[33] G. K. Jarvis, M. Evans, C. Y. Ng, and K. Mitsuke, J. Chem. Phys. **111**, 3058 (1999).
[34] K. Pierloot, B. Dumez, P.-O. Widmark, and B. O. Roos, Theor. Chim. Acta **90**, 87 (1995)
[35] K. Kaufmann, W. Baumeister, and M. Jungen, J. Phys. B **22**, 2223 (1989).
[36] B. O. Roos, K. Andersson, M. P. Fulscher, P.-A. Malmqvist, L. Serrano-Andres, K. Pierloot, and M. Merchan, Adv. Chem. Phys. **69**, 219 (1996).
[37] G. Karlstrom, R. Lindh, P.-A. Malmqvist, B. O. Roos, U. Ryde, V. Veryazov, P. O. Widmark, M. Cossi, B. Schimmelpfennig, P. Neogrady, and L. Seijo, Comput. Mat. Sci. **28**, 222 (2003).
[38] D. R. Yarkony, J. Phys. Chem. A **101**, 4263 (1997).
[39] See supplementary material at http://dx.doi.org/10.1063/1.3652966 for tables of the optimized Cartesian geometries and corresponding harmonic frequencies.
[40] R. Shepard, I. Shavitt, R. M. Pitzer, D. C. Comeau, M. Pepper, H. Lischka, P. G. Szalay, R. Ahlrichs, F. B. Brown, and J. Zhao, Int. J. Quantum. Chem., Quantum. Chem. Symp. **22**, 149 (1988).
[41] H. Lischka, R. Shepard, R. M. Pitzer, I. Shavitt, M. Dallos, Th. Müller, P. G. Szalay, M. Seth, G. S. Kedziora, S. Yabushita, and Z. Zhang, Phys. Chem. Chem. Phys. **3**, 664 (2001)
[42] B. H. Lengsfield III, P. Saxe, and D. R. Yarkony, J. Chem. Phys. **81**, 4549 (1984).
[43] H. Lischka, M. Dallos, P. Szalay, D. R. Yarkony, and R. Shepard, J. Chem. Phys. **120**, 7322 (2004).
[44] Rate constants computed employing extensions to general Franck-Condon integral code originally written by S. Patchkovskii.
[45] E. V. Doktorov, I. A. Malkin, and V. I. Man'ko, J. Mol. Spectrosc. **64**, 302 (1977).
[46] D. Gruner and P. Brumer, Chem. Phys. Lett. **138**, 310 (1987).
[47] F. Zerbetto and M. Z. Zgierski, J. Chem. Phys. **93**, 1235 (1990).
[48] W. Siebrand and M. Z. Zgierski, Chem. Phys. Lett. **58**, 8 (1978).
[49] A. P. Penner, W. Siebrand, and M. Z. Zgierski, J. Chem. Phys. **69**, 5496 (1978).
[50] E. M. Evleth and A. Sevin, J. Am. Chem. Soc. **103**, 7414 (1981).
[51] I. Ohmine, J. Chem. Phys. **83**, 2348 (1985).
[52] M. Barbatti, M. Ruckenbauer, and H. Lischka, J. Chem. Phys. **122**, 174307 (2005).
[53] H. Tao, B. G. Levine, and T. J. Martinez, J. Phys. Chem. A **113**, 13656 (2009).
[54] C. Z. Bisgaard, O. J. Clarkin, G. Wu, A. M. D. Lee, O. Geßner, C. C. Hayden, and A. Stolow, Science **323**, 1464 (2009).